Hardware Calibration of the Modulated Wideband Converter

Etgar Israeli, Shahar Tsiper, Deborah Cohen, Eli Shoshan, Rolf Hilgendorf, Alex Reysenson, Yonina C. Eldar
Technion - Israel Institute of Technology, Haifa, Israel

Abstract—
In the context of Cognitive Radio (CR), opportunistic transmissions can exploit temporarily vacant spectral bands. Efficient and reliable spectrum sensing is key in the CR process. CR receivers traditionally deal with wideband signals with high Nyquist rates and low Signal to Noise Ratios (SNRs). Sub-Nyquist sampling of such signals has been proposed for efficient sampling in CRs. The modulated wideband converter (MWC) is an example of such a sampling scheme. It is composed of an analog front-end, that aliases the signal intentionally before sampling it at a low rate. The signal can then be digitally reconstructed from the low rate samples, using the known relation between the samples and the original signal. Unfortunately, in real hardware implementation, this relation becomes unknown. Physical effects have a considerable impact on the sampling process, and as a consequence, the signal cannot be reliably recovered. In this paper, we present an efficient automated calibration algorithm that builds the actual transfer function of the system, without any prior knowledge. We then present a new, MWC based, CR prototype, on which the calibration algorithm was tested. Experiments on our hardware prototype, based on an embedded proprietary card, show that our calibrated transfer function leads to signal reconstruction whereas the theoretical one fails. Our specification complies with CR requirements of the IEEE standard 802.22 and was experimentally verified with different modulations. It vastly improves a previous prototype in terms of bandwidth, higher maximal frequency and coping with lower SNR.

I. Introduction

In light of the ever-increasing demand for new spectral bands and the under-utilization of those already allocated, the concept of Cognitive Radio (CR) has emerged. Opportunistic users could exploit temporarily vacant bands after detecting the absence of activity of their owners. A crucial task in the CR cycle is therefore spectrum sensing and detection which has to be precise and efficient. Typical CRs deal with wideband signals whose Nyquist rates are very high. Several sub-Nyquist sampling methods have recently been proposed [1], alleviating both the software and hardware burden. Among these systems are the modulated wideband converter (MWC) [2], multi-coset sampling [3] and the random demodulator [4].

This paper focuses on a new MWC prototype implementation for a sub-Nyquist CR system, and its calibration algorithm. In this scheme, after successful calibration, the wideband sparse radio frequency (RF) signal is fed into an analog front-end composed of several hardware channels. In each channel, the signal is mixed with a periodic function that aliases its spectrum, so that each signal portion appears in baseband. The mixed signals are then low-pass filtered and sampled at a sub-Nyquist rate. It is shown in [2] that the low rate samples can be related to the original signal through a linear transformation which depends on the mixing functions. Exploiting this relation, the signal can be recovered digitally from the low rate samples.

In practice, when implementing the MWC, one is faced with hardware issues that alter the relation between the samples and the signal, and prevent signal reconstruction. Such phenomena include non-ideal analog components such as the filters, non-linear effects of the mixers, phase noise and jitter, synchronization issues and more. Due to these effects, the theoretical matrix, that models the transfer function of the system can differ from the one corresponding to the true hardware implementation. We propose an efficient calibration algorithm, completely automated, that can be run once off-line, before using the system, in order to find the effective transfer function. Our approach does not assume any knowledge of the hardware components nor their specifications.

We further present a new MWC hardware implementation which relies on a different technology than previous implementation [1]. Among the new features are: the Nyquist rate of the input signals can be as high as $6GHz$, higher dynamic range, and coping with lower Signal to Noise Ratio (SNR). The reconstruction is performed in real-time from the low rate samples. The novelty of our current implementation is reflected in higher bandwidth for each of the transmitted bands, higher maximal frequency and our proprietary calibration process. All of the system components have been upgraded to support improved dynamic range and real-time reconstruction. The system has been tested with commonly used modulations in communications, and surpasses the requirements of the CR standard, IEEE 802.22 [5].

This paper is organized as follows. In Section II, we present the MWC theoretical background and discuss the motivation behind the calibration process. In Section III, we describe our calibration algorithm. Section IV presents our prototype system specifications. Section V shows hardware simulation results.

II. Background and Motivation

A. The MWC

Let $x(t)$ be a real-valued continuous-time signal, supported on $\mathcal{F} = [-1/2T_{\text{Nyq}}, +1/2T_{\text{Nyq}}]$ and composed of up to N occupied spectral bands, namely $N/2$ real transmissions. The single-sided bandwidth of each transmission does not exceed B. We assume that the carrier frequencies are unknown.

The MWC system [2], described in Fig. 1, is composed of an analog front-end, that aliases the wideband input before

This work is supported in part by the Semiconductor Research Corporation (SRC) through the Texas Analog Center of Excellence (TxACE) at the University of Texas at Dallas (Task ID:1836.114)

978-1-4799-3512-3/14/$31.00 ©2014 IEEE

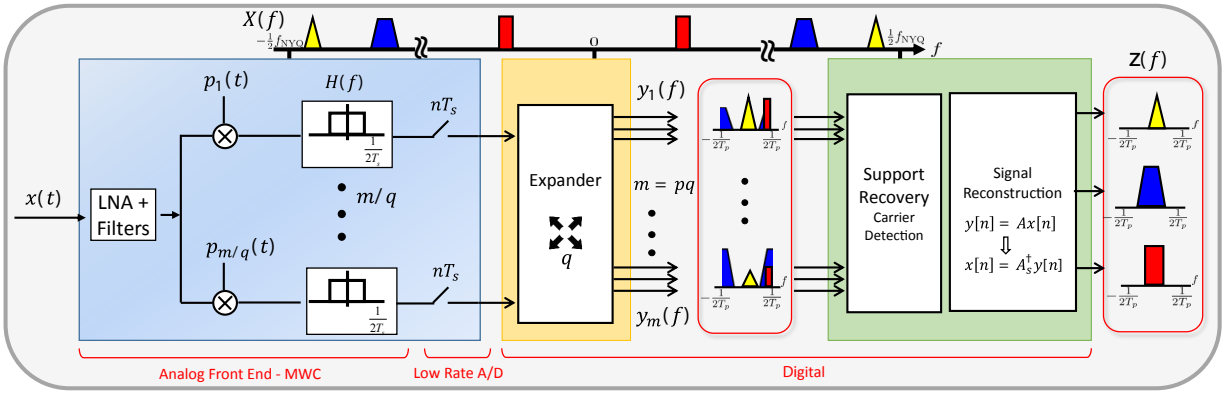

Fig. 1: MWC - cognitive radio analog system and digital processing.

sampling it at a low rate. The following digital processing first recovers the signal's support, namely, the carrier frequencies, and then the signal itself. More precisely, the MWC consists of p channels, that are fed with the input signal $x(t)$. In each channel, an analog mixer mixes $x(t)$ with a $T_p = 1/f_p$-periodic series $p_i(t), (1 \le i \le p)$, such that every portion of the spectrum of $x(t)$ appears in baseband. The mixing series $p_i(t)$ are selected as piecewise constant functions that alternate between the levels ± 1 for each of M equal time intervals. Other choices for $p_i(t)$ are possible, since in principle they are only required to be periodic. The mixed signal is then passed through a low-pass filter with cut-off frequency $1/(2T_s) = f_s/2$ and sampled at the rate $f_s \ge f_p > B$.

The analog process that generates the samples $y_i[n]$ can be modeled using the complex transfer matrix $\mathbf{A}$ as

$$\mathbf{y}[n] = \mathbf{A}\mathbf{z}[n], \tag{1}$$

where $\mathbf{y}[n]$ contains the low rate samples from each channel, and $\mathbf{A}$ is the known matrix containing the Fourier coefficients of the mixing series. The vector $\mathbf{z}[n]$ is unknown and contains the low rate samples of each f_p portion of the spectrum of $x(t)$. Since $x(t)$ is a sparse signal, containing a small number of transmitted bands, most terms of the spectral vector $\mathbf{z}(f)$ are zero. The support is preserved in the time domain samples z[n].

In order to recover $\mathbf{z}[n]$ from the samples $\mathbf{y}[n]$, we first recover its support S using compressed sensing techniques (the reader is referred to [2] for more details). The system can be reduced to that support and solved by

$$\mathbf{z}_S[n] = \mathbf{A}_S^{\dagger}\mathbf{y}[n], \tag{2}$$

where $\mathbf{A}_S^{\dagger}$ denotes the Moore-Penrose pseudo-inverse of $\mathbf{A}$ reduced to the support S. Using the same notation, the vector $z_S[n]$ denotes reducing the vector $z[n]$ to the support S.

Since the matrix $\mathbf{A}$ is constant in time, we can apply a Discrete Time Fourier Transform (DTFT) to both sides of (1) and (2). Rewriting both in frequency produces

$$\mathbf{y}(f) = \mathbf{A}\mathbf{z}(f), \quad \mathbf{z}_S(f) = \mathbf{A}_S^{\dagger}\mathbf{y}(f), \tag{3}$$

where the DTFT of a sequence $x[n]$ is defined as

$$X\left(e^{j2\pi fT}\right) \triangleq X(f) = \sum_{n=-\infty}^{\infty} x[n]\, e^{-j2\pi fTn}. \tag{4}$$

The vector $\mathbf{z}(f)$ containing the spectrum of $x(t)$ divided into f_p slices is defined using the DTFT of $x(t)$ as

$$z_k(f) = X(f + (k - L_0 - 1)f_p), \quad 0 \le k \le L_0, \ f \in \mathcal{F}_p, \tag{5}$$

where,

$$\begin{aligned} f_p &= 1/T_p, \qquad \mathcal{F}_p = [-f_p/2, +f_p/2] \\ f_s &= 1/T_s, \qquad \mathcal{F}_s = [-f_s/2, +f_s/2] \end{aligned} \tag{6}$$

It has been shown in [2] that the minimal number of channels p required is twice the number of occupied bands N. This determines the number of hardware devices (mixers, filters, samplers). Fortunately, the number of channels can be further reduced at the expense of a higher sampling rate $f_s > f_p$ per channel and additional digital processing, referred to as the expander. Basically, each channel sampling at the rate $f_s = qf_p$, with odd expanding ratio $q = 2q' + 1, \ q' \in \mathbb{N}^0$, is equivalent to q channels sampling at rate f_p. Details are given in [2]. The expander transforms the p equations provided by the p physical channels into $m = p \cdot q$ equivalent equations. The recovery process is then identical to the one described above.

B. System Calibration: Motivation

Theoretically, the matrix $\mathbf{A}$ is known and contains the Fourier series coefficients of the mixing series $p_i(t)$ [2]:

$$(\mathbf{A}_{Theory})_{i,l} = c_{il} = \frac{1}{T_p}\int_0^{T_p} p_i(t) e^{-j\frac{2\pi}{T_p}lt}\, \mathrm{d}t. \tag{7}$$

For sequences made of piecewise constant functions, alternating between ± 1, the theoretical matrix can be written as $\mathbf{A}_{Theory} = \mathbf{SFD}$ [2]. Here, $\mathbf{S}_{m\times M}$ is composed from alternating ± 1 values deduced from $p_i(t)$, $\mathbf{F}_{M\times M}$ is the DFT matrix , and $\mathbf{D}_{M\times L}$ is a diagonal complex matrix. This matrix gives 100% support recovery in an ideal MATLAB simulation.

However, in practice, several analog physical effects and imperfections affect the mixing and sampling process, so that the theoretical matrix no longer describes the actual transfer function. In fact, using this matrix on the system prototype failed, even though digital simulations suggest that in perfect conditions this transfer function achieves 100% success rate.

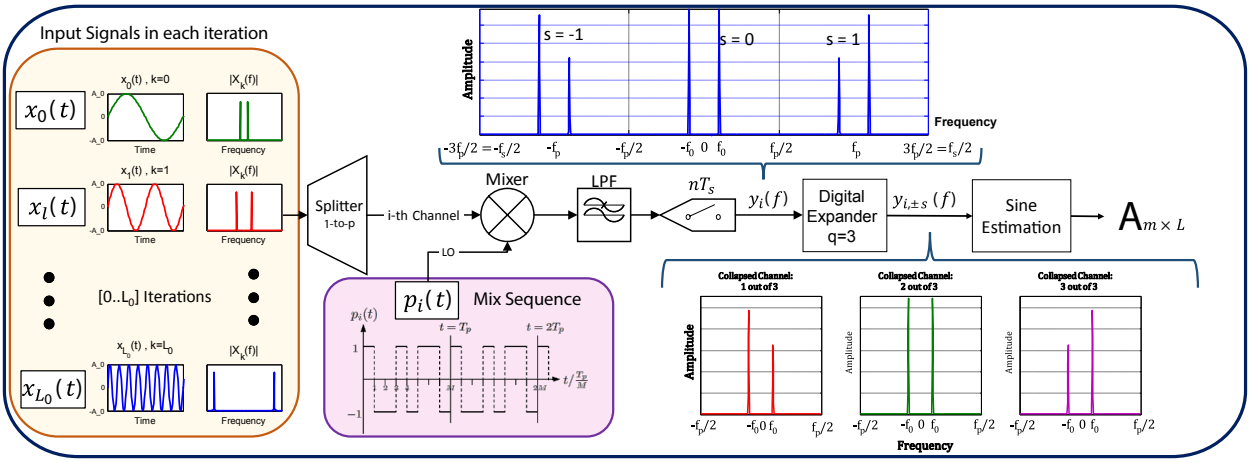

Fig. 2: Single channel diagram, visually showing the calibration process.

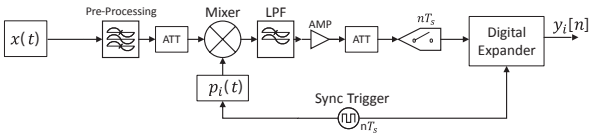

Fig. 3: Single channel diagram that contains filters, amplifiers and attenuators.

This motivates us to calibrate the hardware system in order to discover its actual transfer function.

The main effects that distort the transfer function are:

1) The mixing procedure introduces nonlinearities. Mixers are intended to modulate narrow-band signals with one sine carrier, as opposed to our mixing sequences that effectively contains over a hundred different sine waves.
2) The analog filters have non-ideal response.
3) Actual design uses amplifiers and attenuators. These components exhibit non-linear frequency response.
4) Phase noise and jitter, due to variations in components, cables and clock deltas.
5) Effects of signal-power to noise ratios.

Specifically in our prototype, filters, amplifiers and attenuators are utilized in order to preserve the signal's dynamic range, and prevent saturation or overflow. In addition, the input signal is first processed by an analog module, filtering frequencies below $5f_p$ and above $f_{max} = \frac{f_{Nyq}}{2}$. A single channel diagram can be seen in Fig. 3, showing the added components.

These distortions render the theoretical transfer matrix $\mathbf{A}_{Theory}$ ineffective. An accurate method for estimating the effective $\mathbf{A}$ is crucial to the success of the support and signal reconstruction. To obtain accurate estimation we propose an end-to-end calibration scheme. The proposed procedure, presented in the next section, estimates each of the elements of $\mathbf{A}$, with very little prior knowledge of the mixing series $p_i(t)$ (only their period length T_p), and no knowledge at all about the characteristics of internal system components.

III. Calibration Algorithm

In this section, we describe our calibration algorithm. We first explain the general methodology, and then describe the calibration process for $q = 1$ in detail. Finally, we explain how the process can be altered to fit the general case, including the expander.

A. Calibration Overview

We start by introducing the new notations. The maximal input frequency is defined as $f_{\max} = \frac{f_{\text{Nyq}}}{2} = L_0 f_p$, where $L_0 \in \mathbb{N}$. The transfer matrix is $\mathbf{A}_{m\times L}$, and its terms are denoted by $(\mathbf{A})_{i,l} \triangleq c_{i,l} \in \mathbb{C}$, where $L = 2L_0 + 1$. In addition, let α^* be the complex conjugate of $\alpha \in \mathbb{C}$.

Our goal is to find the MWC transfer function, namely the matrix $\mathbf{A}$, which consists of the Fourier coefficients of the series $p_i(t)$, as defined in (7). Since our system is not time invariant (e.g. samplers), nor linear (e.g. mixers), one cannot find the system transfer function by simply measuring its impulse response. We circumvent this difficulty, by investigating the system's response for every frequency band of the spectrum by injecting consecutive sinusoidal inputs, at incrementing rates.

Algorithm *MWC Calibration*
1. **choose** $0 < f_0 < f_p/2$
2. **for** $l := 1$ **to** L_0 **do**
3. **insert** $x(t)$ - sine with frequency $lf_p + f_0$
4. **for** $i := 1$ **to** p **do**
5. estimate sinusoid parameters $y_i[n]$
6. calculate $c_{i,+l}$ and $c_{i,-l}$
7. **if** $q > 1$ **then**
8. **for** $s := 1$ to $(q-1)/2$ **do**
9. define $y_{\pm}[n] = y_{i+s}[n] \pm y_{i-s}[n]$
10. estimate parameters of y_+ and y_-
11. calculate $c_{i,\pm s,+l}$ and $c_{i,\mp s,-l}$
12. **end for**
13. **end if**
14. **end for**
15. **end for**
16.
(∗ In each iteration of l, produce $2 \cdot q \cdot p = 2m$ coefficients. ∗)

Fig. 5: Calibration algorithm for estimating the matrix $\mathbf{A}$.

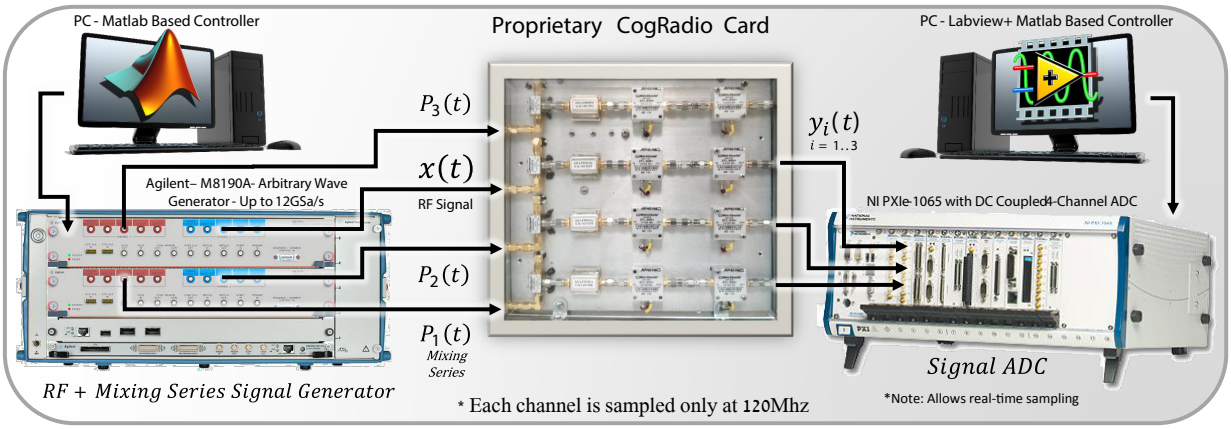

Fig. 4: CogRadio System - Actual Equipment.

B. Calibration method for expansion factor $q = 1$.

We start with a basic system without an expander, comprised of $m = p$ channels and expansion factor $q = 1$. Considering (3), $\mathbf{y}(f)$ denotes the vector of DTFTs of the samples $y_i[n]$ and $\mathbf{z}(f)$ denotes spectrum portions of $x(t)$. Both vectors can be seen in Fig. 1.

For each l iteration we insert the following input signal

$$x_l(t) = \alpha_0 \sin\left[2\pi\left(l f_p + f_0\right) t + \phi_0\right] \ , \ l \quad \in [0, 1, .., L_0]. \tag{8}$$

The parameters α_0 and ϕ_0 can be chosen arbitrarily by the user, while the bias frequency must satisfy $0 < f_0 < f_p/2$. Taking the DTFT of (4) we have

$$X_l(f) = b_0 \delta(f - l f_p - f_0) + b_0^* \delta(f + l f_p + f_0)\,, \tag{9}$$

where $b_0 \triangleq \frac{\alpha_0}{2j} e^{j\phi_0}$. From (5) we then have that for $f \in F_p$

$$\left(\mathbf{z}_l(f)\right)_k = \begin{cases} b_0 \delta(f - f_0 + l f_p), & k = l \\ b_0^* \delta(f + f_0 - l f_p), & k = -l \\ 0, & \forall k \neq \pm l\,. \end{cases} \tag{10}$$

The right hand side of (3) becomes

$$(\mathbf{A}\mathbf{z})_i = c_{i,l}^* \cdot b_0^* \delta(f + f_0) + c_{i,l} \cdot b_0 \delta(f - f_0)\,, \tag{11}$$

which translates in the time domain to

$$(\mathbf{A}\mathbf{z})_i [n] = 2\left|b_0 c_{i,l}\right| \sin\left(2\pi f_0 n T_s + \phi_{i,l}\right)\,. \tag{12}$$

Recalling that (12) is equal to $\mathbf{y}[n]$, we expect a sinusoid wave as output. In practice, the output is a noisy sine, that requires a sine estimation technique, in order to extract $c_{i,l}$. In addition to the added noise, due to non-linear effects of the mixer, the signal contains additional harmonics at DC, and at $k f_p$ and $k f_0$ for $k \in \mathbb{N}$. An example of $y_i[n]$, obtained from our prototype, is presented in Fig. 6.

Following these observations, we model the mixed sampled signal $y_i[n]$ as a random process,

$$\Psi[n] = \sum_k \beta_k \sin\left(2\pi f_k n + \varphi_k\right) + B_0 + u[n]\,. \tag{13}$$

Here, k is used to describe the discrete set of harmonics, B_0 is the DC offset and $u[n]$ is added white noise. The amplitude β_0 is assumed to be the largest, and represents the magnitude of the desired sinusoid at frequency f_0.

Taking the above model into account, we use the following estimation technique, assuming a block of length N_s samples:

1) Remove mean value $\widetilde{\Psi}_n = \Psi_n - \hat{B}_0$, where $\hat{B}_0 = \frac{1}{N_s}\sum_{n=1}^{N_s} \Psi_n$.
2) Use Welch's [6] spectrum estimation to resolve the initial values for the frequency $\tilde{f}_0$, and initial amplitude $\tilde{\beta}_0$, of the strongest sine wave. The frequency $\hat{f}_0$ differ slightly from the known f_0, due to non-linearities of the mixing process.
3) Use the Trust Region Least Squares (TR-LS) [7] method to estimate the phase and improve amplitude estimation. The TR-LS algorithm requires sufficiently close initial values, for which we use the spectrum estimated $\tilde{f}_0$ and $\tilde{\beta}_0$, and solve

$$\left[\hat{\beta}_0, \hat{\varphi}_0\right] = \arg\min_{\beta', \varphi'} \left\| \widetilde{\Psi}_n - \beta' \sin\left(2\pi \tilde{f}_0 n + \varphi'\right) \right\|^2 . \tag{14}$$

Using the estimated parameters we extract the terms $\hat{c}_{i,l}$. Since the functions $p_i(t)$ are real, their respective Fourier transform coefficients satisfy

$$c_{i,-l} = c_{i,l}^* \ , \ \forall i, l\,.$$

After performing $L_0 + 1$ iterations of the above calibration procedure, the matrix $\mathbf{A}$ has been fully built, for positive and negative values of l, column by column:

$$\mathbf{A} = \begin{pmatrix} \hat{c}_{1,-L_0} = \hat{c}_{1,L_0}^* & \cdots & \hat{c}_{1,0} & \cdots & \hat{c}_{1,L_0} \\ \vdots & \ddots & & & \vdots \\ \hat{c}_{i,-L_0} = \hat{c}_{i,L_0}^* & \cdots & \hat{c}_{i,0} & \cdots & \hat{c}_{i,L_0} \\ \vdots & & \vdots & \ddots & \vdots \\ \hat{c}_{p,-L_0} = \hat{c}_{p,L_0}^* & \cdots & \hat{c}_{p,0} & \cdots & \hat{c}_{p,L_0} \end{pmatrix}_{p \times (2L_0+1)} \tag{15}$$

C. Calibration method for expansion factor $q > 1$

We now examine a system comprised of $m = p \cdot q$ expanded channels. For each channel, the expander divides the spectrum of width f_s into $q = 2q' + 1$, $q' \in \mathbb{N}^0$ slices of width $f_p = f_s/q$. Each band is modulated into the base-band and

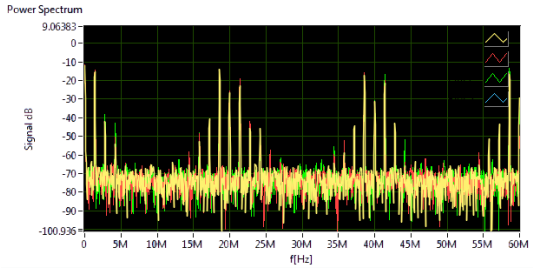

Fig. 6: The modulation of an input signal with the T_p periodic series $p_i(t)$ as the mixer's LO input, adds additional redundant harmonics to the output mixed signal $\mathbf{y}[n]$. When inserting sinusoid waves at rate $kf_p + f_0$ additional harmonics are present at $f = m_1 f_p \pm m_2 f_0,\ m_{1/2}, k \in \mathbb{N}$.

re-sampled at rate f_p, as seen in Fig. 2. Every one of the p physical channel provide q equations in the system (3) after the expander, thus every i-th row of the matrix $\mathbf{A}$ before expansion gives rise to q rows that are cyclic shifted versions of the original one, overall $m = p \cdot q$ rows.

The positive and negative slices of width f_p, once the expander modulates each of them to baseband, contain complex signals, with real and imaginary parts. In order to resolve the transfer matrix terms we can no longer use regular sine estimation methods since each expanded channel does not necessarily contain a sinusoid. Due to lack of space, we only present here the main results for the calibration of a system with a digital expander. Let us define a new index describing for each channel all the slices. The relative slice offset is represented as $s \in [-q', \ldots, 0, \ldots, q']$.

The calibration process still includes $L_0 + 1$ iterations, in which the calibration input signal $x_l(t)$ at iteration l and its coefficients remain as described in (8). Note that for $s = 0$, we get the baseband slice. That slice contains just one real sinusoid, thus we can apply the same treatment as in Section III-B to recover the relevant matrix terms $c_{i,l}$. For $s > 0$, in order to get real signals we use different linear combinations of the slices with indices $\pm s$. This way, we are able to reproduce real sinusoid signals and estimate their respective matrix coefficients $c_{i\pm s,\pm l}$. We repeat this process for each $l \in [0, \ldots, L_0]$ each combination of i and s. By using linear combinations, and conjugate symmetry between the $c_{i\pm s,\pm l}$ terms, we recover all the terms of the expanded $\mathbf{A}_{m\times L}$ matrix, that is fully estimating the system's transfer function.

Figure 5 shows the pseudo code of the derived algorithm.

IV. System Description

We now describe our hardware system prototype, as seen in Fig. 4. The RF input $x(t)$ and the mixing series $p_i(t)$ are generated using the Arbitrary Wave Generator (AWG) - Agilent M8190. The sequences $p_i(t)$ are chosen as Gold Codes [8], which are commonly used in telecommunication (CDMA) and satellite navigation (GPS). Gold sequences were found to give good results in the MWC system, primarily due to small bounded cross-correlations within a set, which is useful when multiple devices are broadcasting in the same frequency range and. Each of the different mixing series are composed from alternating ± 1 values.

	Value	Notes
f_s	120 MHz	$(q+1)\, f_p$ - Sampling rate
f_p	20 MHz	$1/T_p$
q	5	Expansion factor
p	3	# Hardware Channels
$f$max	3 GHz	$f\text{max} = f_{\text{Nyq}}/2$
B	18.5 MHz	Bandwidth on each carrier
M	305	Number of ± 1 intervals in each period of $p_i(t)$

TABLE I: The MWC parameters used in our setup.

In the heart of the system is our proprietary developed MWC card. The card is implemented using connector based analog components, which allows to easily tweak and modify the card characteristics.

Our prototype was fed RF signals with a Nyquist rate of 6 GHz, total maximal bandwidth occupancy of 120 MHz, and varying support into the system. The exact system components used throughout our setup are shown in Fig. 4. The specification of the MWC card is given in Table I.

The digital back-end is implemented using the National Instruments PXIe-1065 computer with DC coupled ADC. Very low computational load is required in order to achieve real time recovery and reconstruction, since all processing is done at the low rate f_p. The matrix $\mathbf{A}$ is calculated once, using the proposed calibration process, and then stored in memory regardless of the input carrier frequencies. MATLAB® and LabVIEW® environments are used to simulate the various digital operations.

V. Calibration Results

We now present the prototype performance using the calibration process. For the sake of comparison, a fully functional, digital, MATLAB implementation of the MWC, was used to emulate an ideal system, i.e. free from the physical difficulties our prototype suffers from, as discussed in Section II-B.

For both systems, we used the parameters defined in Table I. The same Gold sequences, described in the previous section, were selected as the mixing series $p_i(t)$.

For sanity check, we used our calibration process to estimate the transfer function of the MATLAB simulation MWC, and compared the calibrated matrix with the theoretical one. As expected, the MATLAB calibrated matrix also gave 100% support recovery in the ideal MATLAB simulation. A comparison of the theoretical matrix $\mathbf{A}_{Theory}$ versus the MATLAB-calibrated matrix is shown in Fig. 8a. The matrices are nearly identical, demonstrating that the calibration process is successful under digital, ideal, conditions.

We next performed a full calibration, for the actual prototype. A graphical comparison between the calibrated matrix on the prototype, and the theoretical matrix is shown in Fig. 8b. In this case, the two matrices are quite different.

To evaluate the prototype performance, we inserted 1200 noisy RF signals of the form $x(t) + w(t)$, where $x(t)$ is a multiband signal, $w(t)$ is a white Gaussian noise process which is added and scaled so that the test signal has a desired signal-to-noise ratio (SNR). The SNR is defined to be

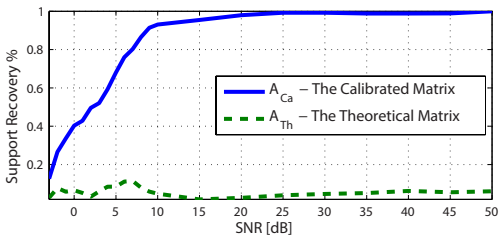

Fig. 7: Hardware reconstruction success % of the calibrated matrix $\mathbf{A}_{Calibrated}$ vs. the theoretical $\mathbf{A}_{Theory}$.

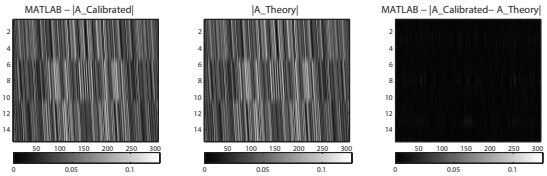

(a) MATLAB Simulation Calibration - Comparison to theory.

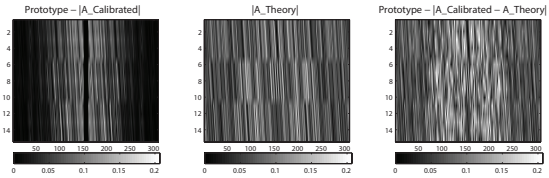

(b) Hardware MWC calibration - Comparison to theory.

Fig. 8: Comparison of the theoretical and the calibrated matrices in MATLAB and hardware environments.

SNR $\triangleq 10\log_{10}\frac{\|x(t)\|^2}{\|w(t)\|^2}$, with the standard ℓ_2 norm. The signal consists of three pairs of bands ($N = 6$), each with bandwidth $B = 18.5Mhz$, containing Phase Shift Keying (PSK) [9], modulated, random data, with energy ratios of $[1, 0.8, 0.2]$. For every signal, the carriers are chosen uniformly at random in $[f_{Nyq}/2, f_{Nyq}/2]$ with $f_{Nyq} = 6Ghz$. The support of the input signal is recovered from a total of 9210 sub-Nyquist samples (3070 for every MWC channel), sampled at only 120 MHz each. The effective system rate is $120 \cdot 3 = 360$ MHz - only 6% of Nyquist. Correct support recovery is defined as the ratio of correct carriers in the estimated support set, out of the entire signal support. Figure 7 shows the percentage of correct support recoveries for various SNR values. The results show that the theoretical matrix failed to recover the signal's support, while the calibrated one accomplished correct recovery above 8 dB SNR.

An example of signal reconstruction can be seen in Fig. 9, which shows the power spectrum of a PSK modulated signal, for SNR $= 25$ dB. The input holds 3 carriers ($N = 6$), each with bandwidth $B = 18.5$ MHz, and carrier frequencies of $[0.92, 1.32, 2.42]$ GHz. The energy ratios were chosen as $[1, 0.8, 0.2]$ respectively. The upper graph shows the input signal power spectrum, the middle one is the MWC output using the prototype-calibrated matrix as the transfer function, and the lower one is the MWC output when using $\mathbf{A}_{\mathbf{Theory}}$ for the support recovery and reconstruction. As can be clearly seen, the calibrated matrix succeeds, while the theoretical one fails.

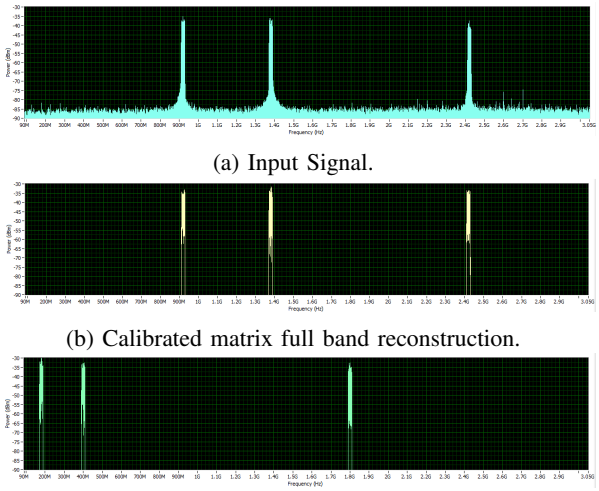

(a) Input Signal.

(b) Calibrated matrix full band reconstruction.

(c) Theoretical matrix full band reconstruction.

Fig. 9: Comparison of signal reconstruction, using the theoretical and the calibrated matrices (hardware simulation).

VI. Conclusion

In this paper, we introduced a calibration method for the hardware implementation of the MWC. Since the theoretical transfer function of the system, modeled by the matrix $\mathbf{A}_{Theory}$, proved ineffective when dealing with real hardware, we propose an automated off-line calibration process. The output is a calibrated matrix $\mathbf{A}_{Calibrated}$ that reflects physical effects and imperfections. With this matrix, reconstruction of the signal is made possible using the hardware prototype.

We simulate scenarii with higher Nyquist rates than those considered in the IEEE 802.22 protocol for CR applications on TV bands, as seen in [5]. We are able to recover those signals from very low rate samples, at only 6% of their Nyquist rate.

References

[1] M. Mishali and Y. C. Eldar, "Sub-nyquist sampling," *Signal Processing Magazine, IEEE*, vol. 28, no. 6, pp. 98–124, 2011.

[2] ——, "From theory to practice: Sub-nyquist sampling of sparse wideband analog signals," *Selected Topics in Signal Processing, IEEE Journal of*, vol. 4, no. 2, pp. 375–391, 2010.

[3] ——, "Blind multiband signal reconstruction: Compressed sensing for analog signals," *Signal Processing, IEEE Transactions on*, vol. 57, no. 3, pp. 993–1009, 2009.

[4] J. A. Tropp, J. N. Laska, M. F. Duarte, J. K. Romberg, and R. G. Baraniuk, "Beyond nyquist: Efficient sampling of sparse bandlimited signals," *Information Theory, IEEE Transactions on*, vol. 56, no. 1, pp. 520–544, 2010.

[5] IEEE-Computer-Society, "Cognitive wireless ran medium access control (mac) and physical layer (phy) specifications," *IEEE Standard-802.22*, July 2011.

[6] P. D. Welch, "The use of fast fourier transform for the estimation of power spectra: a method based on time averaging over short, modified periodograms," *IEEE Transactions on audio and electroacoustics*, vol. 15, no. 2, pp. 70–73, 1967.

[7] J. J. Moré and D. C. Sorensen, "Computing a trust region step," *SIAM Journal on Scientific and Statistical Computing*, vol. 4, no. 3, pp. 553–572, 1983.

[8] R. Gold, "Optimal binary sequences for spread spectrum multiplexing (corresp.)," *Information Theory, IEEE Transactions on*, vol. 13, no. 4, pp. 619–621, 1967.

[9] A. R. Hammons Jr and H. El Gamal, "On the theory of space-time codes for psk modulation," *Information Theory, IEEE Transactions on*, vol. 46, no. 2, pp. 524–542, 2000.